Atomic-scale model for the contact resistance of the nickel-graphene interface

Kurt Stokbro,[*] Mads Engelund, and Anders Blom

QuantumWise A/S and Lersø Parkallé 107, DK-2100 Copenhagen, Denmark

We perform first-principles calculations of electron transport across a nickel-graphene interface. Four different geometries are considered, where the contact area, graphene and nickel surface orientations, and the passivation of the terminating graphene edge are varied. We find covalent bond formation between the graphene layer and the nickel surface, in agreement with other theoretical studies. We calculate the energy-dependent electron transmission for the four systems and find that the systems have very similar edge contact resistance, independent of the contact area between nickel and graphene, and in excellent agreement with recent experimental data. A simple model where graphene is bonded with a metal surface shows that the results are generic for covalently bonded graphene, and the minimum attainable edge contact resistance is twice the ideal edge quantum contact resistance of graphene.

PACS number(s): 72.80.Vp, 73.40.Ns, 73.63.−b

I. INTRODUCTION

Recently, there has been an increasing interest in the use of graphene for electronic devices. One of the outstanding questions is the magnitude of the contact resistance between graphene and metal electrodes since a high contact resistance will limit the performance of field-effect transistors.[1] There have been several experimental investigations of the contact resistance of the metal-graphene interface using four- or two-probe measurements[2–6] and the transfer length method,[3,7] however, currently there is no clear consensus on the value and the dependence of the contact resistance on contact area, temperature, and applied gate potential. Thus, there is a need for complementary theoretical studies, which can give insight about the physical mechanism at play at the metal-graphene interface.

Previous first-principles theoretical studies have focused on the effect of charge transfer between metal and graphene on the contact resistance.[8–11] In this paper, we add knowledge to the understanding of the graphene-metal contact by investigating the effect of covalent bond formation on the contact resistance. We will present quantum transport calculations of the electron transfer from a free suspended graphene sheet to a nickel contact through different metal-graphene contact geometries, where we vary the orientation of the graphene and the contact area between nickel and graphene. Graphene forms a strong covalent bond with nickel,[8] which is similar to the bond formation between graphene and cobalt, palladium, and titanium, thus, the theoretical predictions will also be relevant for these systems. We find that the contact resistance is independent of the orientation of the graphene, as well as of the contact area to the metal, in excellent quantitative agreement with recent experimental observations.[2]

II. CALCULATIONS

Figure 1 illustrates the four different graphene-nickel interfaces considered in this paper. For systems (a), (b), and (c), the graphene is adsorbed on a Ni(111) surface and oriented with a zigzag edge in the transverse transport direction (direction B in Fig. 1). In system (d), it is adsorbed on a Ni(100) surface and has an armchair edge in the transverse transport direction. With this choice of orientation, the lattice mismatch between nickel and graphene is about 1%. In order to simplify the comparison between the different systems, we fix the lattice constant of the graphene, and strain the nickel surface by 1% to obtain a commensurate supercell for both systems. The overlap region between nickel and graphene is 4 Å in systems (a), (c), (d), while it is 8 Å in (b). In (c) and (d), the graphene edge is passivated by hydrogen. Thus, the systems represent very different types of graphene-nickel interfaces.

For the calculations, we have used ATOMISTIX TOOLKIT[12] (ATK), which is a density-functional theory code using numerical localized atomic basis sets. ATK allows for simulating open systems through use of a nonequilibrium Green's function (NEGF) formalism as described in Ref. 13. The systems in Fig. 1 are heterogeneous along the C direction (the left and right electrodes are not the same) and, thus, even at zero bias the system is not periodic in the transport direction. When calculating the electrostatic potential, we therefore employ a Poisson solver, which combines the fast Fourier transform (FFT) method in the A and B directions (in which the structure is periodic) with a multigrid solver for the C direction,[14] where Dirichlet boundary conditions are used for the open system.

We used a double-ζ polarized basis set for expanding the electronic density. This basis set consists of 15 basis orbitals for each nickel atom, with 2 sets of orbitals of s type, 1 of p type, and 2 of d type. The nickel basis functions had an extended range compared to the default ATK basis-set values, in order to obtain a good description of the nickel work function. The radii of the basis functions were 4.46, 4.46, and 2.84 Å for the s, p, and d channels, respectively. For each carbon atom, 13 orbitals per atom were used, with 2 sets of orbitals of s type, 2 of p type, and 1 of d type. The cutoff radius of the orbitals were 2.39, 2.86, and 2.86 Å for the s, p, and d channels, respectively. Other technical parameters were a density mesh cutoff of 150 Rydberg and 9 k points in the B direction where the structures are periodic.

For the exchange correlation, we used the Perdew-Zunger parametrized local spin density approximation[15] (LSDA) since it has been demonstrated to give excellent results for the geometry of the nickel-graphene interface.[16] To determine the geometry of the interface, we first optimized the relative
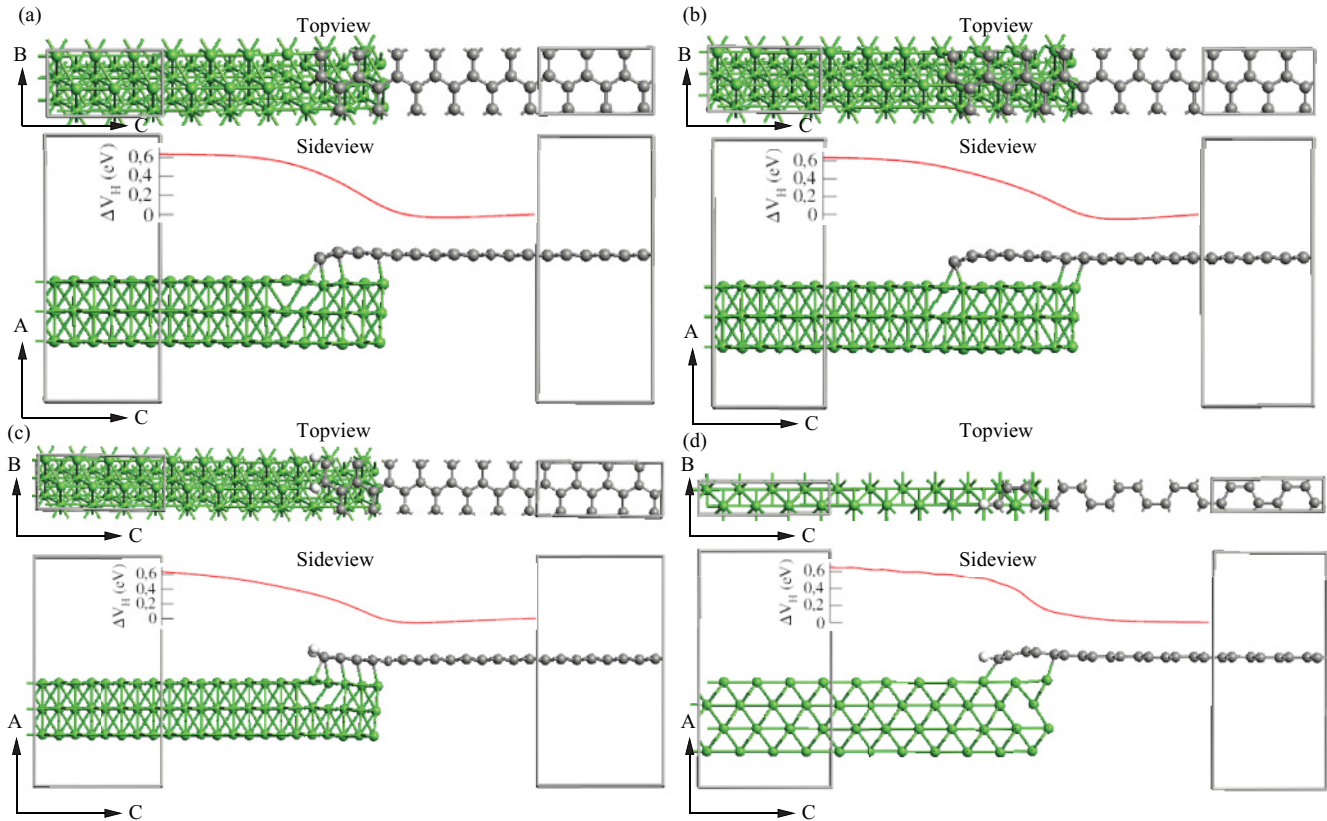
FIG. 1. (Color online) Top view (B-C plane) and side view (A-C plane) of the four systems investigated in this paper. The transport direction is along the C direction. (a) Zigzag edge graphene on top of a Ni(111) surface with 4 Å binding overlap. (b) Similar to (a), but with 8 Å overlap. (c) Similar to (a), but with a hydrogen-passivated terminal edge. (d) Armchair edge graphene on top of a Ni(100) surface with 4 Å overlap, and hydrogen-passivated terminal edge. The inset (red curve) in each figure shows the average electrostatic potential in the vacuum region along the C direction. The potential has been averaged over the B direction for a fixed A coordinate ($A = 18$ Å).

distance between the nickel surface and the graphene layer, with otherwise fixed atom positions. We find a distance of 2.00 Å, in good agreement with Ref. 8. Subsequently, we relaxed all atoms in the interface region such that the force on each atom was less than 0.05 eV/Å.

The relaxed structures are illustrated in Fig. 1. There is a covalent bond formation between the graphene and nickel atoms. The bond formation destroys the π conjugation of the graphene sheet and it is no longer flat, but buckled with distances between the nickel surface and the graphene sheet in the range 1.85–2.3 Å.

Figure 1 also shows the electrostatic profile along the C direction in the vacuum region. We see that the vacuum level is 0.6 eV higher above the nickel surface, compared to the graphene layer, corresponding to a 0.6 eV larger work function W of nickel compared to graphene. This is in excellent agreement with the difference in the measured work function of nickel $W_{100} = 5.22$ eV, $W_{111} = 5.35$ eV,[17] and graphene, $W = 4.6$ eV.[18]

We next calculate the transmission coefficient for each geometry, and the result is illustrated in Fig. 2. We note that the transmission coefficients for the two spin channels are very similar, and the figure therefore only shows the total transmission of both spin channels. For the transmission calculation, we used 501 k points in the B direction. This corresponds

to an equivalent graphene ribbon width of 2134 Å.[9] In the energy range $[-0.1, 0.1]$ eV, the transmission coefficients are almost identical, and have a V-shaped form with a slope
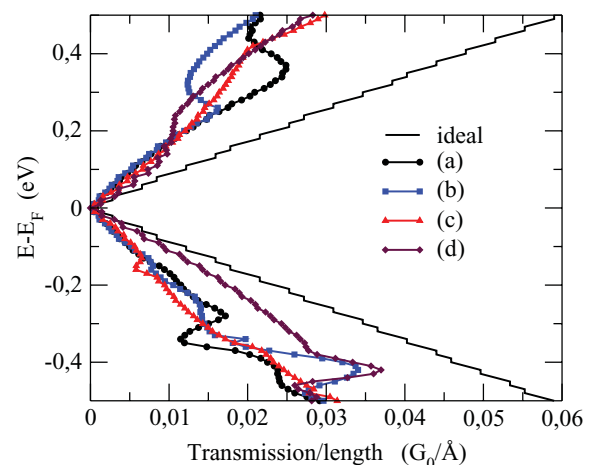

FIG. 2. (Color online) Transmission coefficient per transverse line segment at zero bias for the four different systems illustrated in Fig. 1. Also shown is the transmission coefficient of an ideal graphene layer.
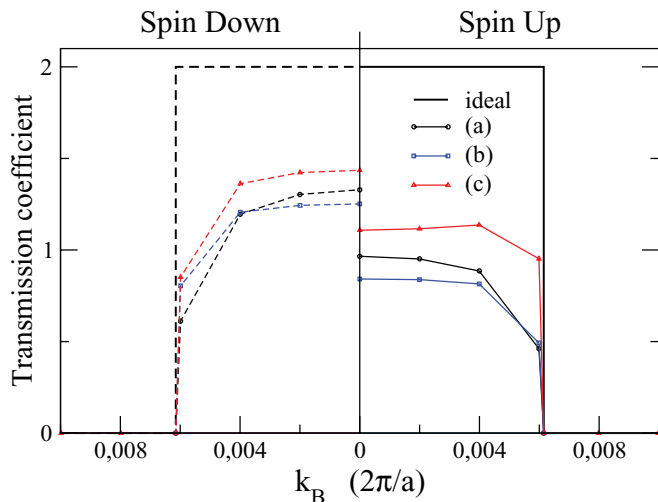
FIG. 3. (Color online) Transmission coefficient at $E = 0.05$ eV as function of the transverse k point in the B direction k_B. The right-hand part of the graph shows the spin-up component, while the left-hand part shows the spin-down component. An ideal graphene sheet has two transmission channels for $k_B < 0.0062 \times 2\pi/a$.
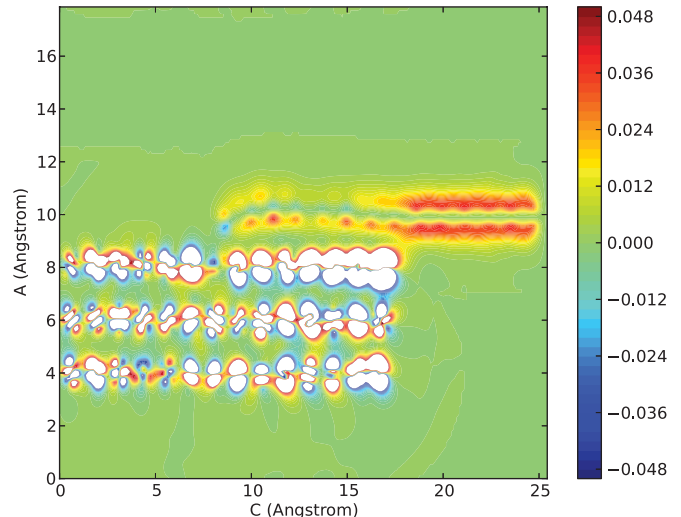

FIG. 4. (Color online) Contour plot of the C component of the linear response current density in the A-C plane for states with energy 0.05 eV, averaged in the B direction (arbitrary units).

$0.06\ G_0/\text{Å eV}$. Figure 2 also shows the transmission of an ideal graphene sheet calculated with the same parameters. Also, in this case the transmission spectrum has the form of a wedge with a singularity at the Fermi level, this time with a slope of $0.12\ G_0/\text{Å eV}$.

Thus, all investigated graphene-nickel systems have a similar contact resistance, which is a factor $\sim$2 larger than the ideal quantum contact resistance of a graphene sheet. In the following, we will analyze the calculations to understand the origin of the similar contact resistance of the four systems.

The transmission coefficient in Fig. 2 is obtained by averaging the transmission coefficient over the k points in the B direction k_B. In Fig. 3, we show how the transmission coefficient varies as function of k_B at the energy $E - E_F = 0.05$ eV. For the perfect graphene sheet, there are two transmission channels for $k_B < 0.0062 \times 2\pi/a$. We see that for systems (a), (b), and (c), approximately half of the channels transmit through the interface, with the total transmission coefficient for the two channels varying in the range 0.8–1.4. Thus, the systems behave qualitatively similar, but there are quantitative differences. It is interesting to note that system (b), which has a larger bonding area than system (a), has a slightly smaller transmission coefficient. Thus, the bonding area does not seem to be an important factor.

To gain further insight into the transport mechanisms, we have also calculated the current density in system (b) (without inclusion of nonlocal potential corrections[19]) from the states with energy 0.05 eV. The result is shown in Fig. 4 and is a real-space view of the current density of the states giving rise to the curve (b) in Fig. 3.

The figure illustrates how the current incident from the right (from the graphene side) gets transmitted through the device. The current density in the graphene layer shows a symmetry corresponding to carbon π electrons carrying the current. The current density in the graphene sheet drops at the boundary between the graphene atoms bonded to the nickel surface and the nonbonded graphene atoms. This means that the main resistance occurs at the interface between nonbonded and bonded graphene atoms, which explains why the bonding area between nickel and graphene is not important.

Figure 5 shows the electrostatic difference potential within the plane of the graphene sheet for the four systems. The plot should be compared with the average electrostatic potential in the vacuum region, illustrated in Fig. 1; note that in Fig. 1 the profiles correspond to a plane far away from the graphene sheet ($A = 18$ Å), whereas in Fig. 5 we cut right through the graphene. The figure also shows the corresponding Mulliken charges $-e(m - z_v)$, where m is the valence Mulliken population of each atom, and z_v is the valence charge. The solid (red) line shows the accumulated charge in the graphene layer.

For all systems, we find that close to the nickel edge, for $C > 15$ Å, there is electron transfer from graphene to nickel, as a result of the 0.6 eV higher work function of the nickel surface compared with graphene. This charge transfer gives rise to a lowering of the electrostatic potential in the graphene sheet. At the edge of the graphene sheet, 10 Å$< C <$ 15 Å, the amount of charge transfer depends on the edge termination. For the nonterminated surfaces (a) and (b), there is an electron accumulation at the edge, corresponding to a negative edge charge. This gives rise to a positive jump in the electrostatic potential. For the H-terminated surfaces (c) and (d), there is an electron depletion at the edge, thus a positive edge charge and a downward jump in the electrostatic potential.

From this, we may conclude that there is no relation between the contact resistance and the charge transfer between nickel and graphene, in contrast with weakly bonded systems where charge transfer has been observed to play an important role.[10]

III. A MODEL SYSTEM

To illustrate that the observed transmission coefficient is rather generic for covalently bonded graphene, we have set up
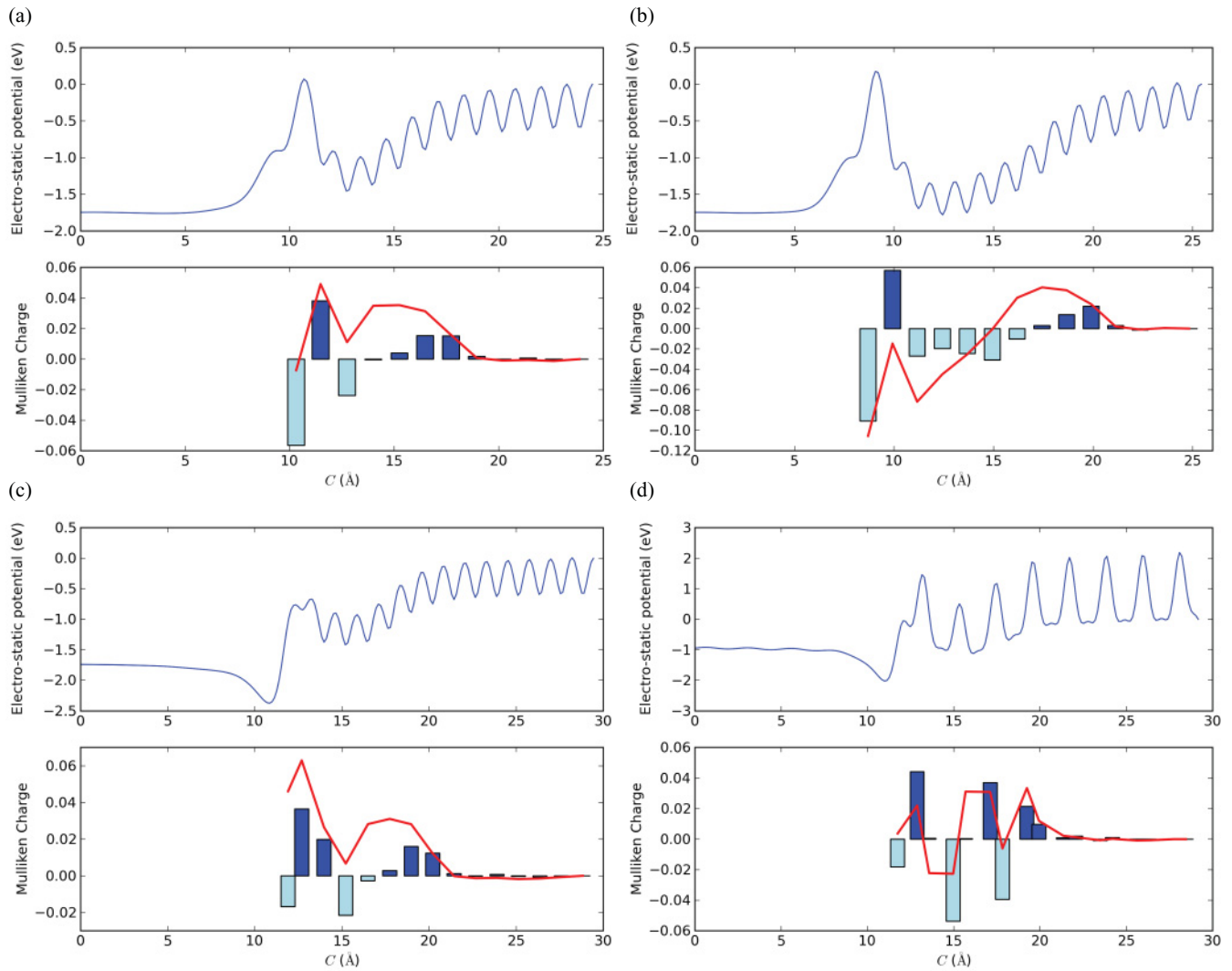
(a)

(b)

(c)

(d)

FIG. 5. (Color online) Average electrostatic difference potential and Mulliken charge inside the graphene sheet plotted along the C direction. Results are shown for each of the four systems in Fig. 1. The electrostatic difference potential is shown for fixed $A = 10$ Å (corresponding to the plane of the graphene sheet) and is averaged over the B direction. The zero point of the potential is defined as the potential at the right-hand edge of the cell. The bar chart shows the Mulliken charge on each atom in the graphene sheet, and the full line shows the accumulated charge from free-hanging graphene to the edge atoms, i.e., the charge is accumulated from right to left.

a simple model system consisting of an aluminum surface and a graphene layer. The system is not relaxed, and the transmission coefficient is calculated using an extended Hückel model.[20] The model in Ref. 20 allows for self-consistently adjusting the onsite elements, but in order to have the most simple model this option is not used in this study.

Figure 6 shows the average transmission coefficient per transverse line segment at the energy $E - E_F = 0.05$ eV as function of the distance between the graphene overlayer and the surface. By varying the adsorption height, we change the effective interaction between the surface and the graphene. The gray area illustrates the variations in the transmission coefficients at this energy for the four systems in Fig. 2. In the range 1 Å$< d <$2.5 Å, there is a strong interaction between graphene and the metal surface, and we see that in this range the transmission coefficient is similar to the systems (a)–(d) in Fig. 2.

Based on these results, we suggest the following model for the electron transmission for a covalently bonded graphene-metal system. The system can be divided into two parts: (i) the nonbonded graphene, and (ii) the metal surface with the covalently bonded graphene. We may now diagonalize system (ii) into left- and right-going modes. When graphene is strongly bonded to the metal surface, we may regard graphene as an extension of the metal surface and there will be equally many left- and right-going modes in the graphene layer. An incoming left-going electron from system (i) may couple with either the left- or right-going modes in system (ii). In the strong-coupling regime, the carbon atoms in system (ii) will be enough perturbed by the metal surface that both left- and right-going modes there bear very little resemblance to the modes in the nonbonded graphene. Thus, the incoming electrons from system (i) will on average have the same coupling strength with left- and right-going modes in system (ii),
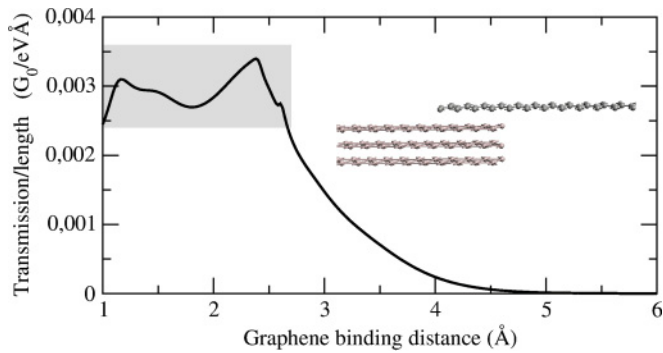
FIG. 6. (Color online) Transmission coefficient per transverse line segment at energy $E - E_F = 0.05$ eV as function of the graphene-surface adsorption distance. Calculations are for a model system consisting of a graphene sheet in contact with a surface made of aluminum. The gray area illustrates the variations of the transmission coefficient per transverse line segment at energy $E - E_F = 0.05$ eV for systems (a)–(d) in Fig. 2.

and thus approximately half of the incoming current is transmitted through the system, as the results in Fig. 2 show.

IV. DISCUSSION

Recent experiments on the contact resistance of the nickel-graphene interface[2] found that the contact resistance did not depend of the contact area, and has an edge contact resistance of ~ 800 Ω μm at room temperature. Our calculations also show that the contact resistance is independent of the contact area. From the transmission spectra in Fig. 2, and the approximation $T(E) \approx 0.06$ (eVÅ)$^{-1}|E - E_F|$, the edge contact resistance can be calculated from

$$1/R = G_0 \times 0.06 \, (\text{eVÅ})^{-1}$$

$$\times \int |E - E_F| \frac{e^{(E-E_F)/k_BT}}{(1 + e^{(E-E_F)/k_BT})^2} \frac{dE}{k_BT}. \quad (1)$$

Using a room-temperature Fermi distribution in the electrodes, we obtain an edge contact resistance of ~ 600 Ω μm. This is in excellent accordance with the experimentally observed value and shows that the contact resistance in the experiment arises from the ballistic quantum contact resistance.

In summary, we have presented calculations demonstrating that the contact resistance of a nickel-graphene junction is independent of the contact area and the direction of the graphene sheet. The edge contact resistance is ~ 600 Ω μm, corresponding to twice the ideal quantum contact resistance of pure graphene and in excellent agreement with experimental data. Additional model calculations predict that this result is generic for strongly bonded graphene on metal surfaces.

*kurt.stokbro@quantumwise.com

[1] F. Xia, D. B. Farmer, Y.-M. Lin, and P. Avouris, Nano Lett. **10**, 715 (2010).

[2] K. Nagashio, T. Nishimura, K. Kita, and A. Toriumi, Appl. Phys. Lett. **97**, 143514 (2010).

[3] A. Venugopal, L. Colombo, and E. Vogel, Appl. Phys. Lett. **96**, 013512 (2010).

[4] P. Blake, R. Yang, S. V. Morozov, F. Schedin, L. Ponomarenko, A. Zhukov, R. Nair, I. Grigorieva, K. S. Novoselov, and A. K. Geim, Solid State Commun. **149**, 1068 (2009).

[5] S. Russo, M. F. Craciun, M. Yamamoto, A. F. Morpurgo, and S. Tarucha, Phys. E (Amsterdam) **42**, 677 (2010).

[6] C. E. Malec and D. Davidovic, Phys. Rev. B **84**, 033407 (2011).

[7] F. Xia, V. Perebeinos, Y.-M. Lin, Y. Wu, and P. Avouris, Nat. Nanotechnol. **6**, 179 (2011).

[8] P. A. Khomyakov, G. Giovannetti, P. C. Rusu, G. Brocks, J. van den Brink, and P. J. Kelly, Phys. Rev. B **79**, 195425 (2009).

[9] S. Barraza-Lopez, M. Vanevic, M. Kindermann, and M. Y. Chou, Phys. Rev. Lett. **104**, 076807 (2010).

[10] J. Maassen, W. Ji, and H. Guo, Appl. Phys. Lett. **97**, 142105 (2010).

[11] Q. Ran, M. Gao, X. Guan, Y. Wang, and Z. Yu, Appl. Phys. Lett. **94**, 103511 (2009).

[12] The transport calculations where performed with ATOM-ISTIX TOOLKIT, version 12.2, [http://quantumwise.com/documents/manuals]

[13] M. Brandbyge, J.-L. Mozos, P. Ordejón, J. Taylor, and K. Stokbro, Phys. Rev. B **65**, 165401 (2002).

[14] T. Ozaki, K. Nishio, and H. Kino, Phys. Rev. B **81**, 035116 (2010).

[15] J. P. Perdew and A. Zunger, Phys. Rev. B **23**, 5048 (1981).

[16] T. Olsen, J. Yan, J. J. Mortensen, and K. S. Thygesen, Phys. Rev. Lett. **107**, 156401 (2011).

[17] B. G. Baker, B. B. Johnson, and G. L. C. Maire, Surf. Sci. **24**, 572 (1971).

[18] C. Oshima and A. Nagashima, J. Phys.: Condens. Matter **9**, 1 (1997).

[19] C. Li, L. Wan, Y. Wei, and J. Wang, Nanotechnology **19**, 155401 (2008).

[20] K. Stokbro, D. E. Petersen, S. Smidstrup, A. Blom, M. Ipsen, and K. Kaasbjerg, Phys. Rev. B **82**, 075420 (2010).